ENSO Signals in Global Upper-Ocean Temperature

YVES M. TOURRE*

Columbia University, Lamont-Doherty Earth Observatory, Palisades, New York

WARREN B. WHITE

University of California at San Diego, Scripps Institution of Oceanography, La Jolla, California

(Manuscript received 24 February 1994, in final form 5 October 1994)

ABSTRACT

The time–space evolution of the El Niño–Southern Oscillation in sea surface temperature (SST) and heat storage of the upper 400 m (HS400) for the Pacific, Indian, and Atlantic Oceans is investigated for 13 years (1979–1991). EOF and rotated EOF (Varimax or VRX) analyses are performed using the time series of normalized anomalies for each ocean separately and then for the global ocean. In the Pacific and Indian Oceans, the two dominant EOF modes for both SST and HS400 are associated with ENSO. For SST they account for 49% of the total variance in each ocean, while for HS400 they account for over 35% of the total variance in each ocean. In the Pacific Ocean, the first EOF modes for SST and HS400 display peak values during spring–summer of 1983 and 1987. They are characterized by maximum positive loadings (or warmer temperature) in the eastern and central Pacific Ocean straddling the equator. These modes represent the peak phase of El Niño off the west coast of South America. The second modes for SST and HS400 are precursor modes with maximum positive loadings in the western and central Pacific Ocean both on and off the equator. The peak values in HS400 second mode lead peak values in HS400 first mode by 6–9 months. Taken together, SST and HS400 first two modes are associated with slow equatorial and eastward propagation of ENSO signals, more clearly though in HS400 than in the SST. In the Indian Ocean, the dominant EOF modes for SST display peak values in summer–fall of 1983 and summer of 1987, while peak values for HS400 are found during fall of 1982 and summer of 1987. Corresponding positive SST loadings are found in the central Indian Ocean while positive HS400 loadings are found in the western Indian Ocean. Maximum values are both straddling the equator. As in the Pacific Ocean, the second EOF modes for SST and HS400 in the Indian Ocean are precursor modes to the first modes. They occur 9–15 months earlier, with warmer SST in the Arabian Sea, colder SST northwest of Australia, and colder HS400 in the vicinity of the boreal winter ITCZ. Taken together, these two modes suggest a slow equatorial and eastward propagation of ENSO signals in SST and HS400, very similar to those in the Pacific Ocean. This propagation can be seen extending eastward south of Indonesia and on into the Timor Sea. There the anomalies have the same sign as the anomalies found in the Philippine and Coral Seas in the western tropical Pacific Ocean during the peak phase of El Niño. In the Atlantic Ocean, ENSO is represented by the third SST VRX mode but not at all in HS400. As such, the Atlantic ENSO signal at the equator is a passive response to a globally perturbed atmosphere. It lags by approximately 18 months the dominant Pacific ENSO mode.

1. Introduction

Initially, El Niño was considered a local climate anomaly of the eastern equatorial Pacific Ocean because of the large fluctuations in sea surface temperature found there every few years (e.g., Enfield 1989). Recognition that El Niño is associated with the Southern Oscillation (Bjerknes 1966a,b, 1969) linked this regional climate phenomenon with one extending over the entire global tropical ocean. The Southern Oscillation had been observed to form a standing wave in the global sea level pressure (e.g., Berlage 1957). Anomalous sea level pressure in the tropical Indian and Atlantic Oceans fluctuate out of phase with their counterpart half a world away in the central and eastern tropical Pacific Ocean. Nevertheless, Barnett (1983, 1984a,b, 1985) found this apparent system of standing oscillation more complicated. He found that the El Niño–Southern Oscillation (ENSO) signal in global sea level pressure and surface winds propagates from the Indian Ocean into the Pacific Ocean. It takes 2–3 years to make the transit (that is at a speed of 10–20 cm s^{-1}). Later, Yasunari (1985, 1987) also observed ENSO signals in sea level pressure and surface wind propagating eastward along the equator at these phase speeds. Yasunari (1987) believed the ENSO signal to

* Current affiliation: Western Connecticut State University, Danbury, Connecticut.

Corresponding author address: Dr. Yves M. Tourre, Lamont-Doherty Earth Observatory, Columbia University, Route 9W, Room 204, Palisades, NY 10964.

be initiated in the Indian Ocean, propagating into and across the Pacific Ocean, and extending into the Atlantic Ocean on an intermittent basis. This suggested to him that eastward propagation of the equatorial ENSO wave from the Indian Ocean influenced the El Niño development in the eastern equatorial Pacific Ocean. More recently, Zebiak (1993) reported evidence that El Niño development in the eastern equatorial Pacific Ocean instigates strong easterly anomalies in the tropical Atlantic Ocean. This in turn leads to the development of contemporaneous negative SST anomalies there.

Meanwhile, observational and theoretical studies of the coupling between ocean and atmosphere (e.g., Zebiak and Cane 1987; Schopf and Suarez 1988; Graham and White 1988) have suggested that the ENSO can be explained quite adequately from coupled dynamical principles confined to the Pacific Ocean. This involves adherence to those principles embodied in the delayed action oscillator of the Pacific Ocean (Suarez and Schopf 1988) that involve the reflection of ENSO Rossby waves at the western boundary and the slow eastward propagation of coupled ENSO waves along the equator. The dominance of the Pacific Ocean dynamics upon El Niño development is also indicated with prediction studies by Latif and Graham (1992) and others. They achieve remarkable El Niño forecasting capability from consideration of coupled ocean–atmosphere models confined to the Pacific Ocean only. Still, the Southern Oscillation is a global tropical phenomenon, affecting both the Indian and Atlantic Oceans as well as the Pacific Ocean. The possibility that the Indian Ocean may have an influence upon ENSO phenomenon in the Pacific Ocean, as suggested by Yasunari (1985, 1987) and others, must be explored.

In the present study, we examine interannual ENSO signals in upper-ocean temperature anomalies in the Indian, Pacific, and Atlantic Oceans for 13 years (1979–1991). We chose sea surface temperature and heat storage in the upper 400 m (HS400) as indicators of interannual variability of temperature in the upper ocean. Empirical orthogonal functions and rotated EOF analyses are used to characterize the space–time evolution of ENSO. This follows on the heels of the earlier work of White et al. (1985), White et al. (1987), and Graham and White (1988). They used EOF analyses of SST and vertically averaged temperature anomalies to characterize the 1982–83 and 1986–87 El Niño activity in the tropical Pacific Ocean. On the other hand, Nitta and Yamada (1989) and Kawamura (1994) examined global SST of EOF and rotated EOF, respectively. In our analysis, leading SST EOF and rotated EOF modes are found very similar to those in earlier studies. We examine the dominant modes that characterize ENSO in all three oceans separately both at the surface (SST) and to a depth of 400 m (HS400). The modes that represent ENSO in the Indian and Atlantic Oceans are compared with the Pacific ENSO modes. We also examine EOF modes for the entire global tropical ocean, allowing the phase relationships between ENSO in the three different oceans to be determined.

2. Observations and methods

This study utilizes monthly anomalies of sea-surface temperature (SST) and heat storage in the upper 400 m (HS400) over much of the global ocean. They are based upon the global distribution of available temperature profiles for the period mentioned above. Representative geographical distributions for 1985 as well as monthly sampling for the entire period are displayed in Fig. 1. Approximately 3000–6000 observations per month were collected during the first 10 years of this 13-year record, with about half this number (i.e., 1000–3000 observations per month) collected during the last three years of the record. This reduction in sampling density occurs because of the 2–3 year delay in the submission of many of the temperature profiles to the National Oceanographic Data Center, from where these observations come. The sampling density is uneven in space as well, with the North Pacific Ocean and the North Atlantic Ocean displaying the highest sampling densities. Sampling densities are smaller in the tropical oceans, greater in the Pacific than in the Indian and Atlantic Oceans, and virtually nonexistent in the Southern Hemisphere oceans poleward of approximately 30°S.

The largest portion of the 662 000 available temperature profiles collected during the 13-year period is composed of expendable bathythermograph (XBT) profiles (that is, 91%). The XBT measures temperature from a thermister as the probe falls through the water column with a known fall rate from which depth is derived by measuring time. XBT probes are deployed principally from the Ship Of Opportunity (SOO) program operated by the Tropical Ocean–Global Atmosphere (TOGA) and the World Ocean Circulation Experiment (WOCE) programs under the auspices of the Integrated Global Ocean Services System (IGOSS). These temperature profiles have been subjected to rigorous quality control procedures defined under guidelines of the Global Temperature–Salinity Project (GTSP). Details of the quality control procedures are given in White et al. (1988).

Analyses are conducted upon the time sequence of mapped estimates of SST anomalies and HS400 anomalies. Both of these anomaly variables are mapped objectively (Gandin 1963) from the location of the original temperature observations onto a 2° latitude by 5° longitude grid each month, over as much of the global ocean as possible for the period considered in this study. The objective mapping is configured to grid for the least-dominant scales of variability (i.e., 2° latitude, 4° longitude, 2 months, and a noise-to-signal

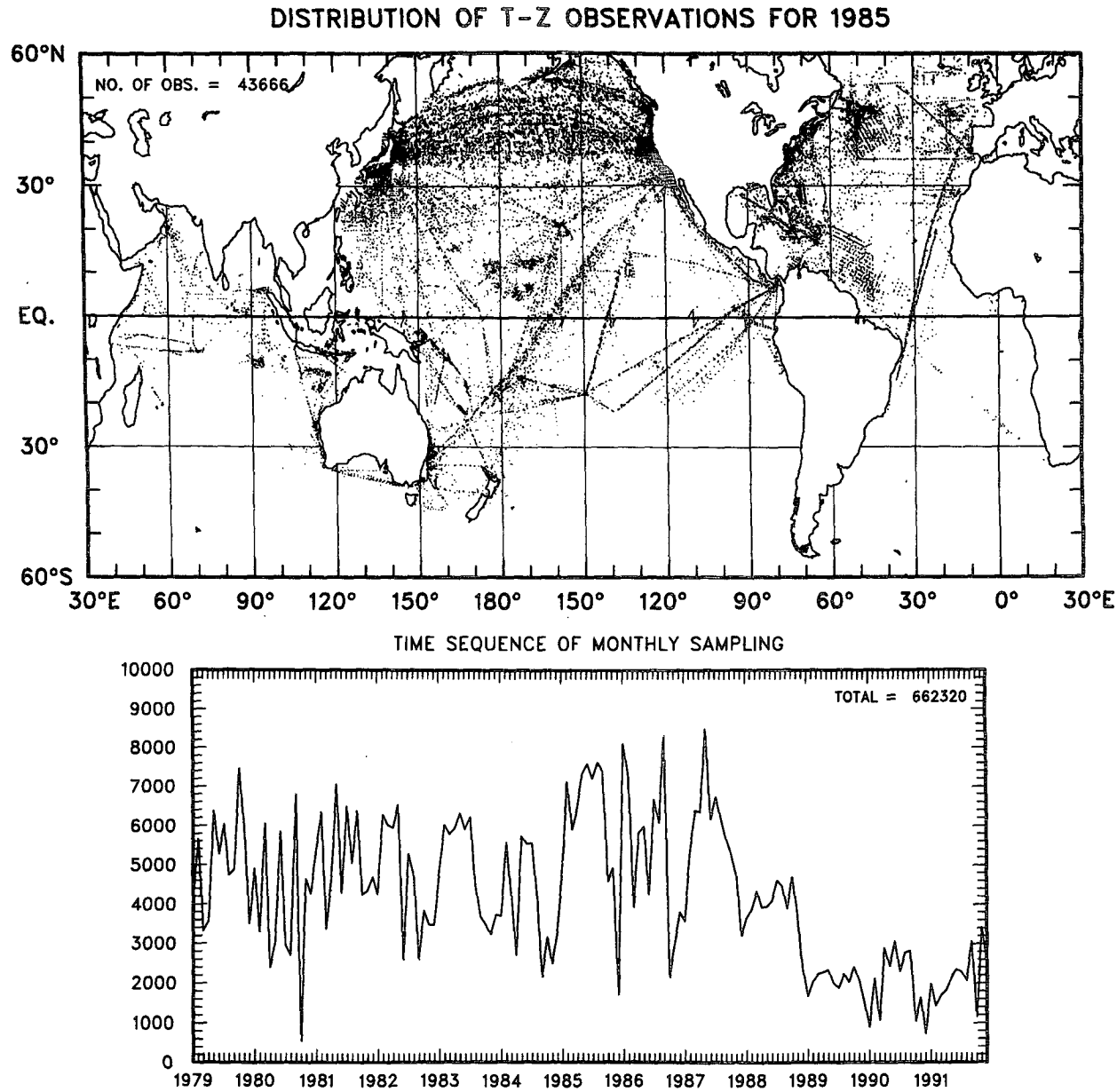

FIG. 1. Top: distribution of temperature profiles over the global ocean, used in the construction of temperature anomalies for 1985. The decorrelation timescale being 3 months means that observations from ±3 months on either side from the middle of each month were used in the computation of anomalies. Bottom: number of monthly profiles available for the present study.

ratio of 1.0), interpolating the upper ocean temperature anomalies onto a regular grid (i.e., 2° latitude, 4° longitude, 1 month) for the 13 years. The search distance for selecting observations about each grid node are ±5° latitude, ±10° longitude, and ±3 months. As an example, the normalized interpolation error at the surface for June 1985 is given in Fig. 2, as the best that can be expected for the period. The map of normalized errors in Fig. 2 displays the smallest errors (i.e., less than 0.75) in the middle latitude North Pacific Ocean north of 40°N, off the east and west coasts of North America, and along repeated transects through the tropical Pacific Ocean. These locations are where the sampling densities over the global ocean were largest (Fig. 1). Larger errors occur where sampling density is less dense or absent altogether. This produces errors that range from 0.7 to 0.9 of the signal standard deviation over most of the global ocean where routine sampling occurs (i.e., 30°S–60°N).

Anomalies are the differences of individual temperature estimates from the climatological monthly mean. The latter is computed over a 10-year base period from

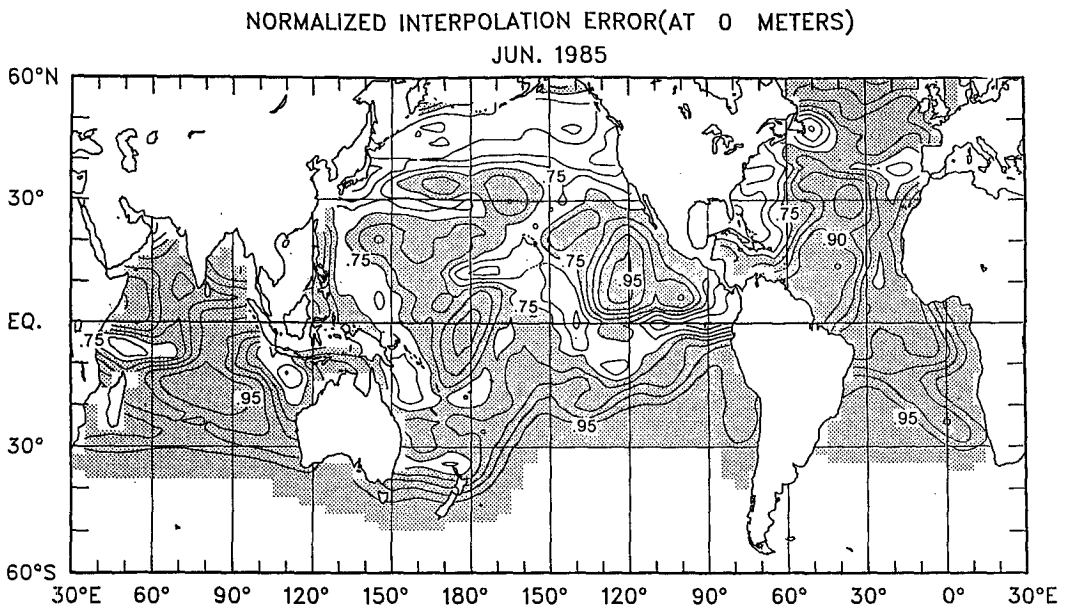

FIG. 2. Map of normalized interpolation error for June 1985 at the surface. Units are in standard deviation of the signal. The regions with largest errors are shaded (i.e., larger than 0.75 of the signal standard deviation). Contour every 0.05 standard deviation of the signal.

1979 to 1988. This period is chosen as the base period primarily because the distribution of the temperature profiles is relatively uniform during this time. However, anomalies are computed for the 13-year period, using this base period of 1979–1988 as the reference. As such, the anomalies do not sum to zero over the entire period.

Global distributions of the annual mean SST and HS400 for the base period 1979–1988 are displayed in the upper panels of Figs. 3 and 4. Major features of the mean SST (Fig. 3, top) include cold water tongues penetrating to the equator along the eastern boundaries of the Atlantic and Pacific Oceans as well as the "warm pool" (Wyrtki 1989) in the equatorial eastern Indian and western Pacific Oceans where SST is above 28°C. The thermal equator is a major feature (SST above 27°C) located beneath the intertropical convergence zone (ITCZ) near 8°N in the Pacific and Atlantic Oceans. Warm temperatures can also be found in the western South Pacific Ocean under the South Pacific convergence zone (SPCZ). Major features of the mean HS400 (Fig. 4, top) include representations of the shallow tropical gyres in the Pacific, Atlantic, and Indian Oceans, as HS400 is proportional to the relative geopotential anomaly and to the relative sea level height. In the North Pacific, North Atlantic, and South Indian, and South Pacific Oceans near 8°N and 8°S, troughs associated with eastward flowing countercurrents on their equatorward sides are well identified.

Global distributions of the standard deviation of the anomalous SST and HS400 for the 13-year period are displayed in the lower panels of Figs. 3 and 4. Major features of the standard deviation of the SST anomalies (Fig. 3, bottom) include maxima (minima) in the equatorial regions of the eastern (western) Pacific, the eastern (western) Atlantic, and the western (eastern) Indian Oceans. Major features of the standard deviation of the HS400 anomalies (Fig. 4, bottom) include maxima in the eastern and central equatorial Pacific Ocean, in the western tropical North Indian Ocean, and in the western tropical North Atlantic Ocean. Interesting differences occur in the western boundaries of the North Pacific and North Atlantic Oceans, with the maximum in the former being zonally distributed and that in the latter being more meridionally distributed.

EOF analysis is used to examine the time series of SST and HS400 anomaly maps for the 13-year period (i.e., 157 maps for each variable). We compile both EOF and rotated EOF (Varimax criterion, VRX hereafter) analyses. Prior to the analysis the time series at each grid point are filtered by using a recursive low-pass (18-month half power) filter (Kaylor 1977). Due to the extensive latitudinal extent of the gridded fields, a metric factor for appropriate scaling [i.e., (cosine of latitude)$^{1/2}$] is also applied to the EOF correlation matrix following North et al. (1982). EOF analysis permits the compression of any time sequence of horizontal maps when a few of the uncorrelated spatial patterns are found to account for most of the variance in the dataset. However, results from EOF analysis may be subject to misrepresentation because of the constraint of orthogonality placed upon the spatial modes (i.e., the eigenvectors). Indeed higher modes may have an unrealistic predictable geometric relationship to the first mode, particularly when that mode dominates strongly.

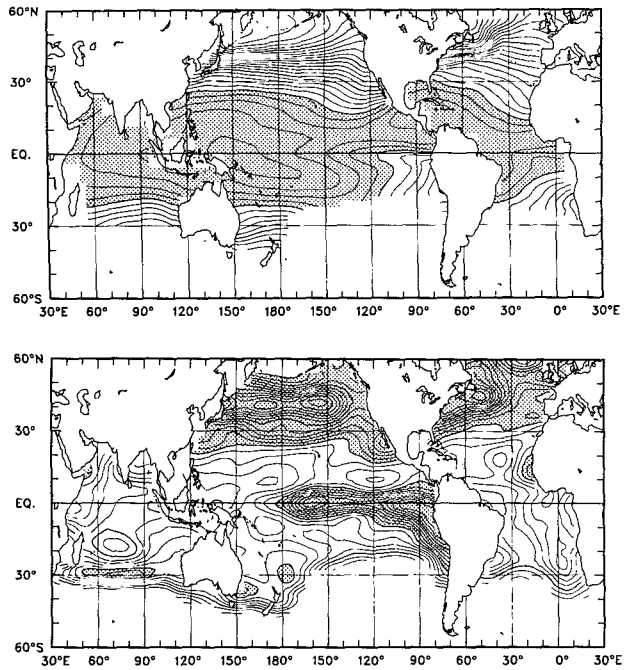

FIG. 3. Top: annual long-term mean of the SST over the global ocean for the reference period 1979–1988. Values greater than 25°C are stippled. Contour every 1°C. Bottom: Standard deviation of the SST anomalies over the global ocean for the 13-year period of interest from 1979 to 1991. Values greater than 0.5°C are stippled. Contour every 0.05°C.

When the EOF modes are rotated using VRX, the spatial orthogonality condition is relaxed in favor of the maximization of the variance of the squared correlations between the modes and the original time series at each grid point (Kaiser 1958). This procedure also simplifies the loading distribution. The VRX method and its applications are well described in the literature (e.g., Horel 1981; Richman 1986). A cumulative variance of 75% is used as the threshold that determines the number of EOF to be kept, prior to rotation. Area weighting is also considered when the rotation is applied to the EOF modes, following Davis (1973). We find that, in the Pacific and the Indian Oceans, by conducting the EOF analysis, the scaling, and the VRX rotation, the highly ranked VRX modes do not differ significantly from the leading EOF modes. The dominant modes in the Pacific and Indian Oceans are then truly orthogonal in space. This is also true for the global ocean modes, where it will be shown that the Pacific and Indian Oceans dominate. This is not the case in the Atlantic Ocean due to the degeneracy of the leading EOF modes following North et al. (1982). A similar result was obtained by Houghton and Tourre (1992). Consequently, in the Atlantic Ocean and global analyses, only rotated modes (VRX) will be considered.

In the following, the regions where positive (negative) loadings are found correspond to a warm (cold) phase in the upper ocean. These regions and time periods of the warm phases are shaded throughout the figures. Peak values refer to the ENSO warm phase and are associated with the extreme positive values of the amplitude functions. Extrema of the spatial structures are either dark shaded (warmest) or stippled (coldest).

3. ENSO signals in the Pacific Ocean

The EOF analysis in the Pacific is conducted independently of those in the other two oceans. The EOF amplitude functions (time sequences, hereafter) of the first two EOF modes for SST and HS400 normalized anomalies in the Pacific Ocean are displayed in Figs. 5 and 6. For SST (mode 1) and HS400 (modes 1 and 2) the ENSO signal is clearly seen in these time sequences, with positive values or peaks near 1982–83 and 1986–87.

The time sequence for the first EOF mode of SST, explaining almost 33% of the total variance, displays major peaks in the spring–summer of 1983 and the summer–fall of 1987 (Fig. 5, top). The time sequence for the first EOF mode of HS400, explaining 24% of the total variance, displays major peaks at the same times as in the first mode of SST (Fig. 6, top). These first EOF modes in SST and HS400 represent the peak

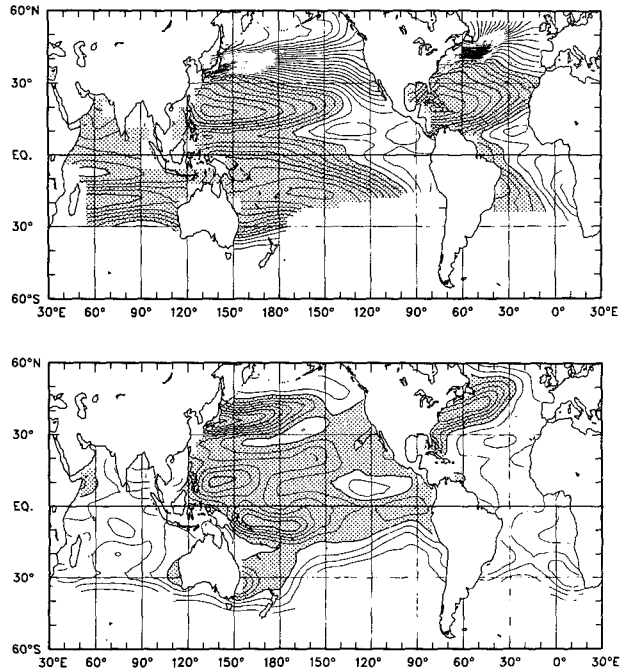

FIG. 4. Top: Annual long-term mean of the heat storage in the upper 400 m (HS400) over the global ocean for the reference period 1979–1988. Values greater than 6×10^5 cal cm^{-2} are stippled. Contour every 0.2×10^5 cal cm^{-2}. Bottom: Standard deviation of the HS400 anomalies over the global ocean for the 13-year period of interest from 1979–1991. Values greater than 2×10^4 cal cm^{-2} are stippled. Contour every 0.2×10^4 cal cm^{-2}.

phase of El Niño in the eastern equatorial Pacific Ocean. The time sequence for the second EOF mode of SST, explaining 17% of the total variance, displays mostly positive values from 1980 until spring of 1982 (with a brief period of negative values at the end of 1981), from summer of 1985 until fall of 1987 (with extremely small values during the first half of 1987), and from summer of 1989 on to the end of the record (Fig. 5, bottom). The first two periods lead peak values in the first mode in SST. A high-frequency signal (in the vicinity of 2 years) is apparent in the second mode time sequence. That this signal is modulated at longer timescales, as suggested by Ropelewski et al. (1992), complicates the estimation of the lead time, since ENSO peaks are not easily identifiable. The time sequence for the second mode of HS400, explaining 17% of the total variance, displays major peaks in the fall–winter of 1982 and the spring of 1987 (Fig. 6, bottom). The peaks in the time sequence of HS400 second mode lead peaks in the time sequence of the HS400 first mode by 6–9 months. The large values at the end of the record are not representative since this is the time when the number of observations dropped considerably (Fig. 1, bottom). The same remark also applies to the end of SST second mode time sequence.

The spatial structure of the first EOF mode for SST (Fig. 7, top) has positive loadings in the central and eastern equatorial Pacific Ocean, extending along the west coast of North America. Maximum values are found along the equator from the west coast of Central America westward to the date line. The negative loadings, which are organized in a V-shape fashion, extend from west of 160°E at the equator to 30°N and 20°S. This pattern, when associated with the corresponding peaks in the time sequence, represents the canonical spatial structure in SST associated with peak phase of El Niño off the west coast of South America (Rasmusson and Carpenter 1982). The spatial structure of the first EOF mode for HS400 (Fig. 8, top) has positive loadings in the eastern equatorial Pacific Ocean, extending along the west coast of North America, with two tongues protruding westward along 18°N and 5°S. Maximum negative loadings are found at the equator centered around 160°E and along the climatological position of the SPCZ. This pattern, during the periods of peak values in the time sequences, also represents the canonical spatial structure in HS400 associated with El Niño off the west coast of South America (White et al. 1985). The negative HS400 loadings in the western equatorial Pacific Ocean are poised to propagate eastward along the equator, operating to terminate the El Niño over the subsequent year's time. The relationship between SST and HS400 in these first modes is very similar to that observed by Graham and White (1988), where maximum positive loadings of HS400 are displaced to the east of maximum positive loadings of SST.

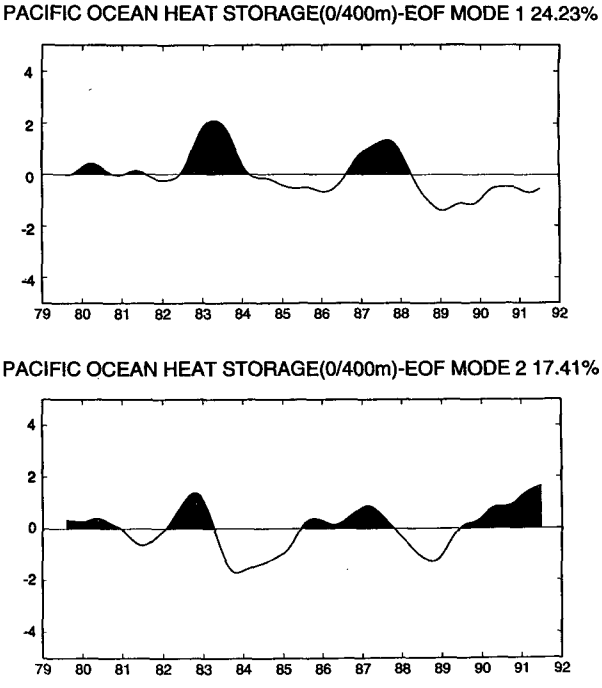

FIG. 6. Time sequences of the first two EOF modes for HS400 normalized anomalies over the Pacific Ocean for the 13-year period 1979–1991. Positive values including peaks are shaded. Units are standard deviation. The tick marks refer to 1 Jan. of each year.

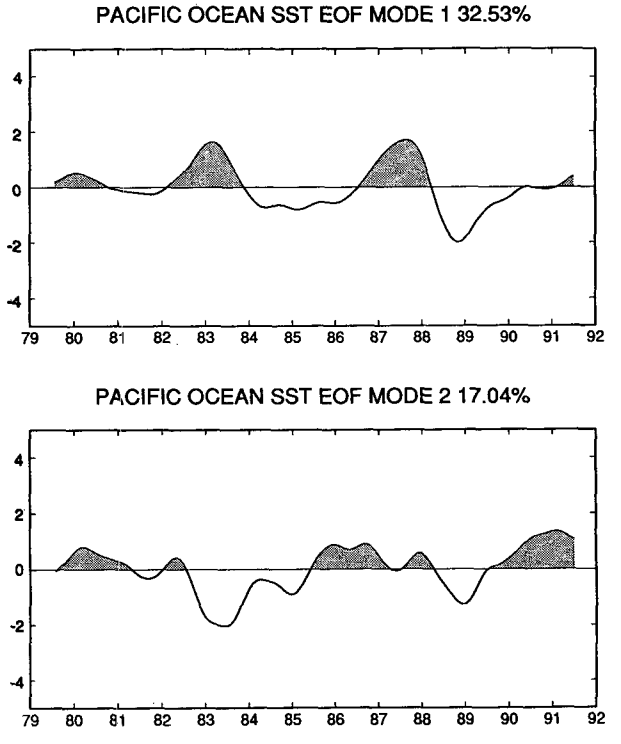

FIG. 5. Time sequences of the first two EOF modes for SST normalized anomalies over the Pacific Ocean for the 13-year period 1979–1991. Positive values including peaks are shaded. Units are of standard deviation. The tick marks refer to 1 Jan. of each year.

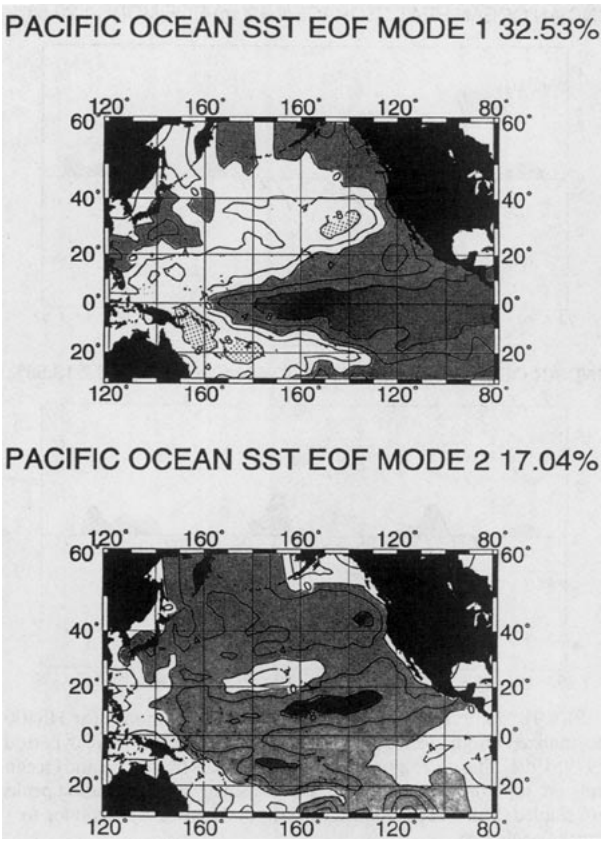

FIG. 7. Spatial patterns (loadings ×10) of the first two EOF modes for SST over the Pacific Ocean for the 13-year period 1979–1991. Areas with positive values are shaded. Extrema of the same order of magnitude are either dark shaded (positive) or stippled (negative).

The spatial structure of the second EOF mode for SST (Fig. 7, bottom) is dominated by positive loadings. Maxima extend along the Equatorial Currents on the poleward flanks of the climatological ITCZ and the SPCZ (see Fig. 3, top). To the north, between 10°N and 20°N, warmer SST, found at least 6–9 months prior to the peak phase of El Niño, may be due to weakened westward advection of cold water by the Equatorial Currents. The spatial structure of the second EOF mode for HS400 has negative loadings on the northern flank of the ITCZ. This also indicates a weakening of the North Equatorial Current (consistent with warmer SST in the same region). Positive HS400 loadings (or warmer temperature 6–9 months prior to the peak phase of El Niño) in this second EOF mode can be found in the central and eastern Pacific Ocean, straddling the equator and around 45°N between 135°W and the date line. When the spatial structures of SST and HS400 second modes for the tropical Pacific Ocean are compared, it is found that SST positive loadings (warmer temperature) tend to be displaced westward of HS400 positive loadings (warmer temperature) and away from the equator.

In summary, the first EOF modes of both SST and HS400 characterize the peak phase of El Niño off the west coast of South America. Maximum positive loadings occur in the central and eastern Pacific Ocean straddling the equator. The second EOF modes for both SST and HS400 are precursor modes to the first EOF modes. When warmest SST is found in the vicinity of the ITCZ and SPCZ off the equator, warmest HS400 is found contemporaneously at the equator, from 130°W until 170°W. The leading peak values of HS400 time sequence occur 6–9 months prior to the canonical El Niño surface structure. The first and second EOF modes for HS400, taken together are associated with slow eastward propagation of the ENSO signal along the equator and westward propagation off the equator (e.g., Gill and Rasmusson 1983; White et al. 1985; Kessler 1990). The first and second modes for SST, taken together, yield a much weaker sense of eastward propagation along the equator. An equatorward propagation of the anomalies is nevertheless suggested and is equivalent to a merging of the ITCZ and SPCZ along the equator (Pazan and Meyers 1982).

4. ENSO signals in the Indian Ocean

The EOF analysis in the Indian Ocean is conducted independently of those in the other two oceans. Time sequences of the first two EOF modes for SST and HS400 anomalies in the Indian Ocean are displayed in Figs. 9 and 10. For each parameter, the ENSO signal

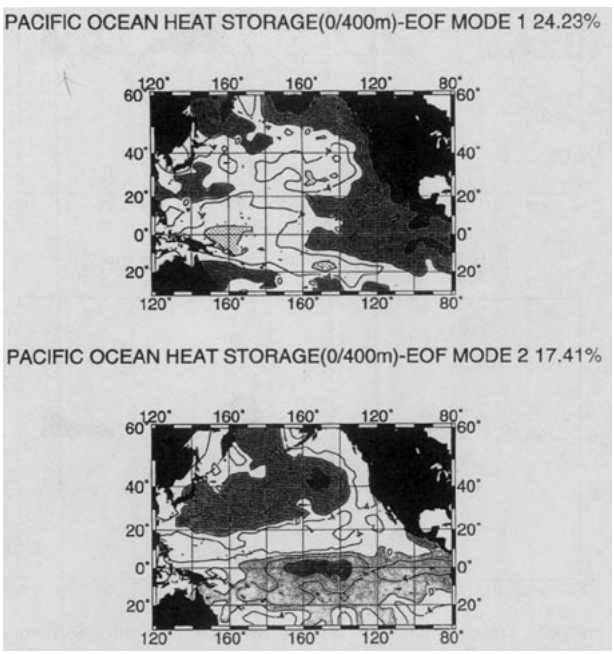

FIG. 8. Spatial patterns (loadings ×10) of the first two EOF modes for HS400 over the Pacific Ocean for the 13-year period 1979–1991. Areas with positive values are shaded. Extrema of the same order of magnitude are either dark shaded (positive) or stippled (negative).

can be seen in these time sequences, with peaks near 1982–83 and 1986–87, similar to those seen in Figs. 5 and 6 for the Pacific Ocean.

The time sequence for the first EOF mode of SST, explaining almost 31% of the total variance, displays major peaks in the summer–fall of 1983 and the summer of 1987 (Fig. 9, top). The first peak in the Indian Ocean lags by approximately 6 months the first peak in the Pacific Ocean while the second peaks are in phase in both oceans (compare the two time sequences displayed in Fig. 9, top). The time sequence for the first mode of HS400, explaining almost 21% of the total variance, displays major peaks in the fall of 1982 and the summer of 1987 (Fig. 10, top). This leads the first mode for peak SST in 1983 but is in phase with the 1987 peak SST. The HS400 first mode time sequence is almost in phase with that of the HS400 first mode in the Pacific ocean since the peaks of 1982 are slightly offset (compare the two time sequences displayed in Fig. 10, top). The time sequence for the second EOF mode of SST, explaining almost 18% of the total variance, displays positive values throughout 1981–82 and 1986–87, with peak values during summer of 1986 (Fig. 9, bottom). The positive values during 1981–82 and 1986–87 lead peak values in the first mode of SST.

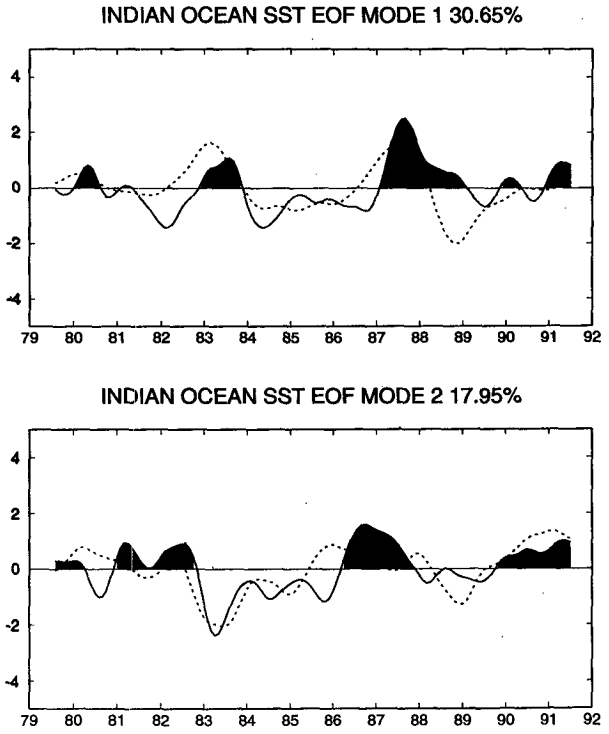

FIG. 9. Time sequences of the first two EOF modes for SST normalized anomalies over the Indian Ocean for the 13-year period 1979–1991. The corresponding time sequences for the Pacific Ocean only are superimposed as dashed lines. Positive values including peaks are shaded. Units are standard deviation. The tick marks refer to 1 Jan. of each year.

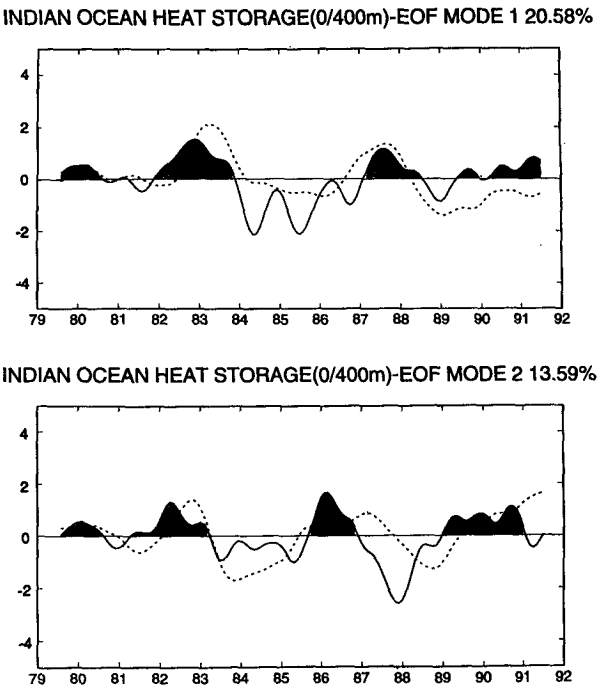

FIG. 10. Time sequences of the first two EOF modes for HS400 normalized anomalies over the Indian Ocean for the 13-year period 1979–1991. The corresponding time sequences for the Pacific Ocean only are superimposed as dashed lines. Positive values including peaks are shaded. Units are standard deviation. The tick marks refer to 1 Jan. of each year.

A 12-month peak to peak lead time is noticeable during the 1986–87 ENSO event. The apparent low-frequency signal in that same time sequence is approximately in phase (except 1980 and 1985) with the second mode of SST in the Pacific Ocean (compare the two time sequences displayed in Fig. 9, bottom). The time sequence for the second mode of HS400, explaining 14% of the total variance, displays major peaks during winter of 1981/82 and spring of 1982 and during winter of 1985/86 and spring of 1986, with positive values throughout 1989–90 (Fig. 10, bottom). The peaks of the time sequence of HS400 second mode lead approximately by 9 to 15 months peak values of the time sequence of HS400 first mode and by approximately 6 to 12 months the peak values of the time sequence of the Pacific HS400 second mode.

The spatial structure of the first EOF mode for SST (Fig. 11, top) has positive loadings throughout the central and northern Indian Ocean (i.e., the Arabian Sea and the Bay of Bengal) with maximum values centered at the equator. Accordingly, warmer SST is found in these same regions during summer–fall of 1983 and summer of 1987, while colder SST is found northwest of Australia. This corresponds to the Pacific SST first mode where positive loadings are found in the central and eastern Pacific Ocean straddling the equator. The spatial structure of the first EOF mode for HS400 (Fig.

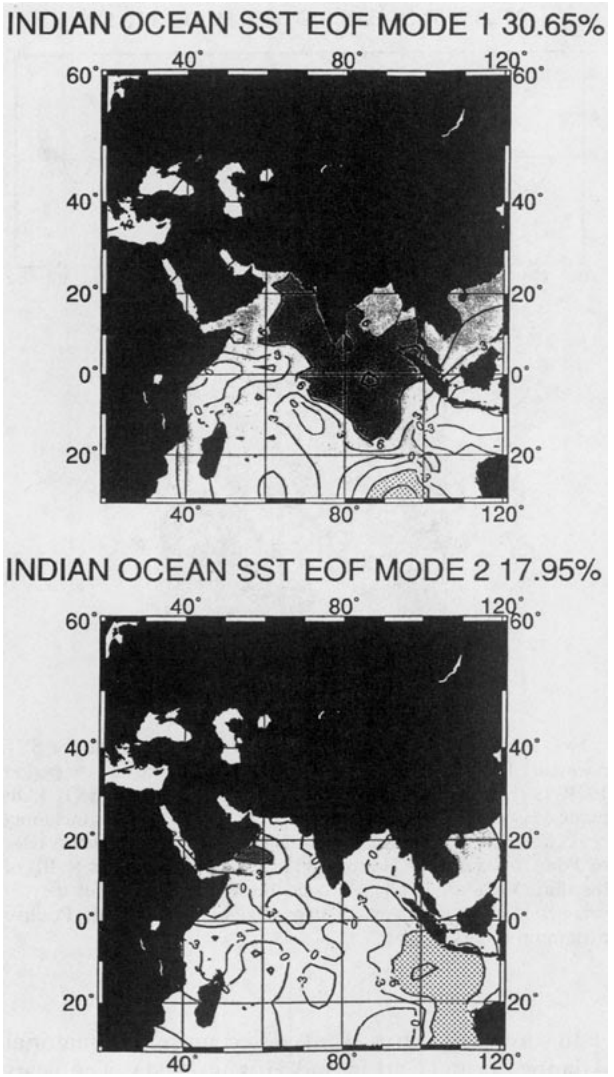

FIG. 11. Spatial patterns (loadings × 10) of the first two EOF modes for SST over the Indian Ocean for the 13-year period 1979–1991. Areas with positive values are shaded. Extrema of the same order of magnitude are either dark shaded (positive) or stippled (negative).

12, top) has positive loadings in the western Indian Ocean, west of 85°E with maximum at the equator extending northward into the Arabian Sea. Maximum negative loadings of the same magnitude are found in the Bay of Bengal, South China Sea, the Greater Sunda Islands, and northwest of Australia. This corresponds to the Pacific HS400 first mode with positive loadings in the eastern Pacific Ocean straddling the equator and negative loadings in the regions of Papua New Guinea and the Solomon Islands. Therefore, the relationship between SST and HS400 in the Indian Ocean in the first mode is very different from that in the Pacific Ocean where SST positive loadings tend to be displaced westward of the HS400 positive loadings (Figs. 7 and 8, top). In the Indian Ocean, SST positive loadings tend to be displaced eastward of HS400 positive loadings (Figs. 11 and 12, top).

The spatial structure of the second EOF mode for SST (Fig. 11, bottom) has positive loadings in the northwestern sections of the ocean (i.e., the Arabian Sea), with maximum loadings along the Saudi Arabia peninsula. Negative loadings are found everywhere else, with maxima in the southeastern Indian Ocean (i.e., the northwest Australia Basin). This corresponds to the Pacific SST second mode with maximum positive loadings in the western and central Pacific Ocean and small negative loadings in the extreme western Pacific Ocean (i.e., Coral and Arafura Seas, Fig. 7, bottom). The spatial structure of the second EOF mode for HS400 (Fig. 12, bottom) is largely dominated by negative loadings. The largest values, which occur during winter–spring, are found on the poleward side of the boreal winter Indian Ocean ITCZ. Small positive loadings are confined to the Somali Basin, the northwest Arabian Sea, and the Timor Sea. This spatial structure precedes by 12–18 months the first mode of HS400 in the Pacific Ocean with positive loadings in eastern Pacific Ocean straddling the equator (see Fig. 8, top).

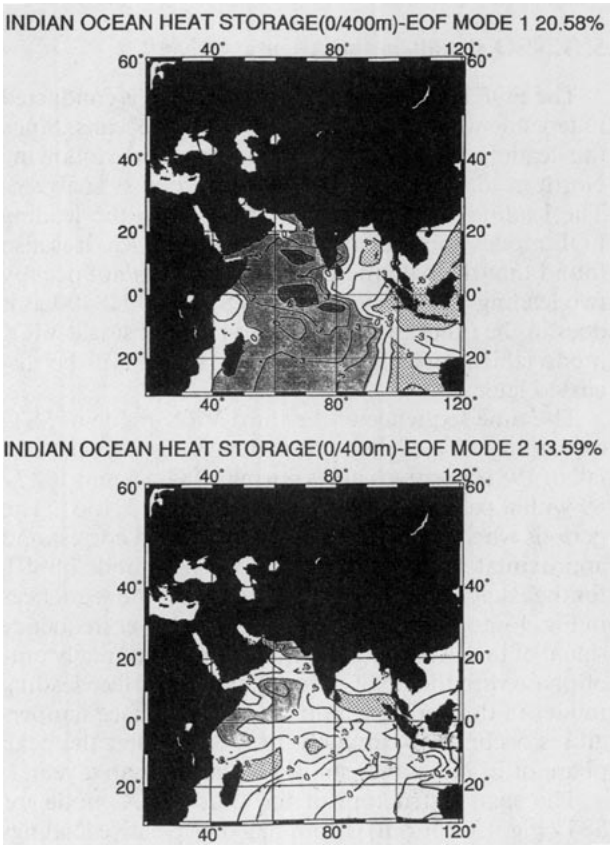

FIG. 12. Spatial patterns (loadings ×10) of the first two EOF modes for HS400 over the Indian Ocean for the 13-year period 1979–1991. Areas with positive values are shaded. Extrema of the same order of magnitude are either dark shaded (positive) or stippled (negative).

In summary, the first EOF modes of both SST and HS400 characterize the ENSO signal in the Indian Ocean. While maximum warmer SST and HS400 occur in the central and eastern equatorial Pacific Ocean during the peak phase of El Niño, warmer SST and HS400 occupy the central and western equatorial Indian Ocean. As in the Pacific Ocean, the second EOF modes for both SST and HS400 in the Indian Ocean are precursor modes, which occur 9–15 months earlier than the first modes. Warmer SST appear first in the Arabian Sea extending to the Central and southeastern Indian Ocean approximately 12 months later, with maxima found at the equator. In the subsurface colder HS400 occurs first, during winter–spring along the ITCZ location, and is found 9–15 months later in the extreme eastern Indian Ocean and western side of the warm pool. This is also the time when the western Indian Ocean is dominated by warmer HS400. Taken together, these two modes for SST and HS400 are associated with the slow eastward propagation of the ENSO signal along the equator in the Indian Ocean, extending in the eastward, southeastward direction along the southern coast of Indonesia and on into the Timor Sea. Negative HS400 loadings seem to be trapped in the Bay of Bengal.

5. ENSO signals in the Atlantic Ocean

The EOF analysis in the Atlantic Ocean is conducted independently of those in the other two oceans. Since the leading EOF modes are degenerated, following North et al. (1982), VRX modes are also analyzed. The leading VRX modes do differ from the leading EOF modes and are not orthogonal in space. It is also found that the Atlantic ENSO signal does not occupy two leading VRX modes in both SST and HS400 as it does in the other two oceans, but rather a single VRX mode (third mode) for SST only, which will be discussed later.

The time sequence of the third VRX mode of SST, explaining 13% of the total variance, displays peak in fall of 1981, positive values during 1984–85 and 1987–89 with a peak during spring 1989 (Fig. 13, top). The periods when positive values are displayed correspond approximately to the troughs in the first mode of SST for the Pacific Ocean (compare the two time sequences in Fig. 13, top). This indicates that the lower frequency signal of that Atlantic SST mode is approximately out-of-phase with the ENSO surface and subsurface leading modes in the Pacific Ocean. Warmest surface temperatures occur approximately 18 months after the peak phase of El Niño and can last for more than a year.

The spatial structure of the third VRX mode for SST (Fig. 13, bottom) is dominated by positive loadings with maxima in the central equatorial Atlantic. This is the region where Kawamura (1994), in a global analysis, found an "isolated oscillatory mode" (fourth rotated mode).

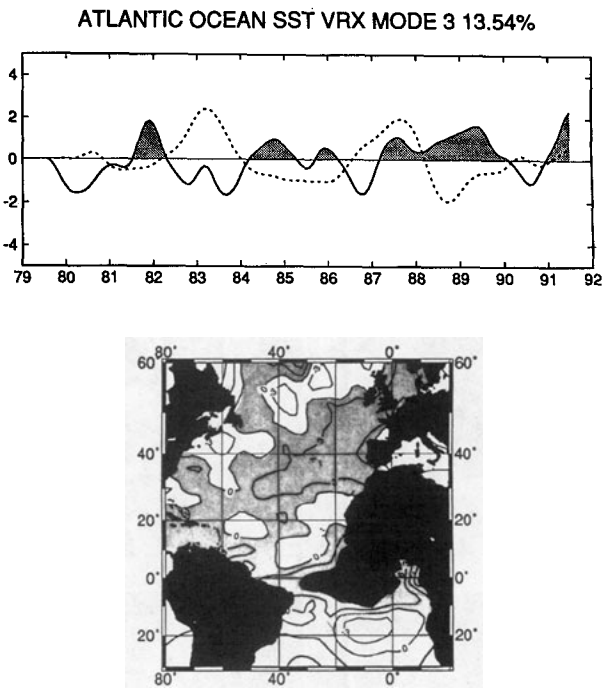

FIG. 13. Top: time sequences of the third VRX mode for SST normalized anomalies over the Atlantic Ocean for the 13-year period 1979–1991. The time sequence for the Pacific Ocean (SST, EOF mode 1) is superimposed (as dashed line). Positive values including peaks are shaded. Units are standard deviation. The tick marks refer to 1 Jan. of each year. Bottom: spatial patterns (loadings × 10) of the third VRX mode for SST over the Atlantic Ocean for the 13-year period 1979–1991. Areas with positive values are shaded. Positive extremum is dark shaded.

In summary, warm events do occur in the equatorial Atlantic ocean (Carton and Huang 1994). The years 1984 and 1988–89 are the warmest years during the analyzed period. The unusual conditions during 1984 are well described by Philander (1986). It has been suggested that this particular warm event was associated with the remnant of a deep thermocline in the west occurring after the ENSO 1982–83 (Houghton and Colin 1986; Carton and Huang 1994). A similar conclusion cannot be reached for the 1988–89 warm event. This may rely upon the fact that the phase relationship between SST and the depth of the 20°C isotherm in the tropical Atlantic fluctuates with latitude and that the phasing can reverse itself along the equator (Houghton 1991). Moreover, the ENSO signal in the Atlantic Ocean does not seem to have an easily discernible evolution at the surface and subsurface, as it does in the Pacific and Indian Oceans. Consequently, zonal propagation resulting from the interaction of two modes in a quadrature phase at the surface and subsurface appears not to be a priori a characteristic of the ENSO signal in the Atlantic Ocean. Mechanisms for Atlantic warm events have been suggested by observing

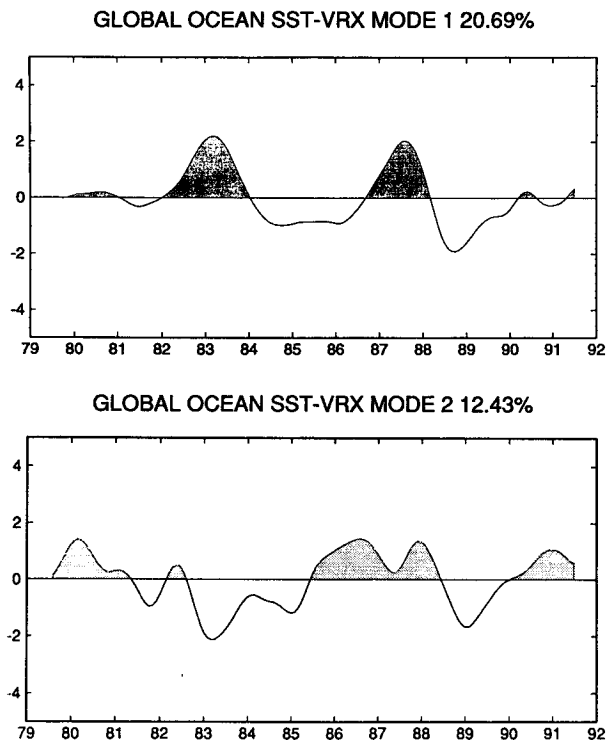

FIG. 14. Time sequences of the first two VRX modes for SST normalized anomalies over the global ocean for the 13-year period 1979–1991. Positive values including peaks are shaded. Units are standard deviation. The tick marks refer to 1 Jan. of each year.

the work of Katz et al. (1986) and more recently by the modeling study of Zebiak (1993). These authors found a tendency for the southeasterly trade winds of the Atlantic Ocean to increase during the peak phase of El Niño when the sea level pressure is minimum in the eastern Pacific. This intensification of the trades induces cold SST anomalies to form over the equatorial and southeast tropical Atlantic Ocean in response to increased local sensible and latent heat fluxes, anomalous equatorial upwelling and cold advection by the South Equatorial Current. The equatorial Atlantic warm events then occur after the relaxation of the southeasterly trade winds and the reinforcement of the North Equatorial Counter Current during the year following the Southern Oscillation index (SOI) minima (Katz 1993). This occurs approximately 18 months after the fully developed Pacific El Niño. In addition, in the Atlantic as opposed to the Pacific, the tropical SST interannual variability cannot be attributed only to local equatorial ocean–atmosphere coupling, which is insufficiently strong as demonstrated by Zebiak (1993). This suggests that in the Atlantic Ocean, south of the ITCZ, there are periods when the equatorial interannual SST variability (13% of the total variance) represents a passive response to atmospheric eastward perturbation, ENSO induced, and originating in the Indo-Pacific region.

6. ENSO signal over the Global Ocean

The EOF analysis applied to the global ocean is principally concerned with defining the spatial patterns of the ENSO signal in the Indian and Atlantic Oceans that have covariance with the spatial patterns of the ENSO signal in the Pacific Ocean. Since the leading Atlantic EOF modes are degenerated, only the global VRX modes are discussed.

The resulting time sequences of the first two VRX modes for SST and HS400 over the global ocean are displayed in Figs. 14 and 15. For each variable, the ENSO signal can be seen in these time sequences, with peak values near 1982–83 and 1986–87. Comparison of these time sequences with those for the Pacific Ocean (Figs. 5 and 6) finds them to be nearly identical. This is because the Pacific Ocean constitutes approximately 70% of that portion of the global ocean considered in this study. Therefore, interannual variability in the Pacific Ocean does dominate the global interannual variability in this analysis.

The time sequence for the first VRX mode of SST, explaining almost 21% of the total variance, displays major peaks in the spring of 1983 and the summer of 1987 (Fig. 14, top). The time sequence for the first VRX mode of HS400, explaining 16% of the total variance for the global ocean, displays major peaks at the same times as in the first mode of SST (Fig. 15, top). Both of these first VRX modes in SST and HS400

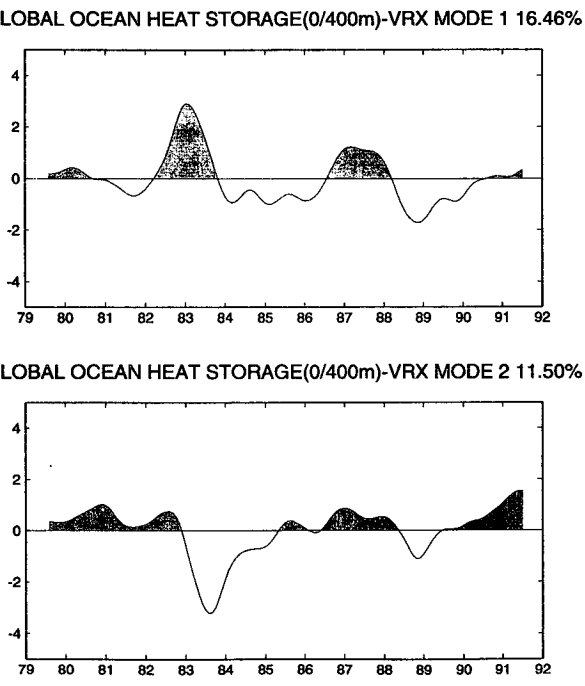

FIG. 15. Time sequences of the first two VRX modes for HS400 normalized anomalies over the global ocean for the 13-year period 1979–1991. Positive values including peaks are shaded. Units are standard deviation. The tick marks refer to 1 Jan. of each year.

represent the peak phase of El Niño in the eastern equatorial Pacific Ocean. The time sequence for the second VRX mode of SST, explaining 12% of the total variance for the global ocean, displays positive values starting prior to the peak summer–fall values of the first SST mode and lasting for at least 18 months. These periods lead peak values in the time sequence of the SST first mode by at least 6 months. The time sequence for the second VRX mode of HS400, explaining 11% of the total variance, displays positive values throughout 1980–82, 1985–87, and after 1990 (Fig. 15, bottom). The first two periods lead peak values in the first mode of HS400.

The spatial pattern of the first VRX mode for SST over the global ocean (Fig. 16, top) has positive loadings in the central and eastern equatorial Pacific Ocean, with maximum values extending from the west coast of South America westward to the date line. This pattern represents the canonical spatial structure in SST associated with the peak phase of El Niño off the west coast of South America (Rasmusson and Carpenter 1982). Of principal interest are the positive SST loadings straddling the equatorial Indian Ocean and the positive loadings in the Atlantic Ocean north of the ITCZ and around 55°N, while negative loadings are found between the equator and 10°S. This pattern in the Indo-Pacific regions goes hand in hand with the peak phase of El Niño off the west coast of South America. It is very similar to the pattern displayed by the first VRX mode obtained by Kawamura (1994) using unfiltered data with no spatial scaling. The only difference is in the westward shift (toward the Caribbean) of the maximum loadings found in the northern tropical Atlantic. By contrast the pattern in the Atlantic somewhat resembles the third VRX mode of Kawamura (1994), which he associated with a "dominant decadal time scale variability." Note that south of Indonesia and in the Timor Sea, the SST loadings are of the same sign as the SST anomalies in the Coral and Philippine Seas of the western tropical Pacific Ocean. This may be indicative of an atmospheric teleconnection between the Indian and Pacific Oceans. Note also

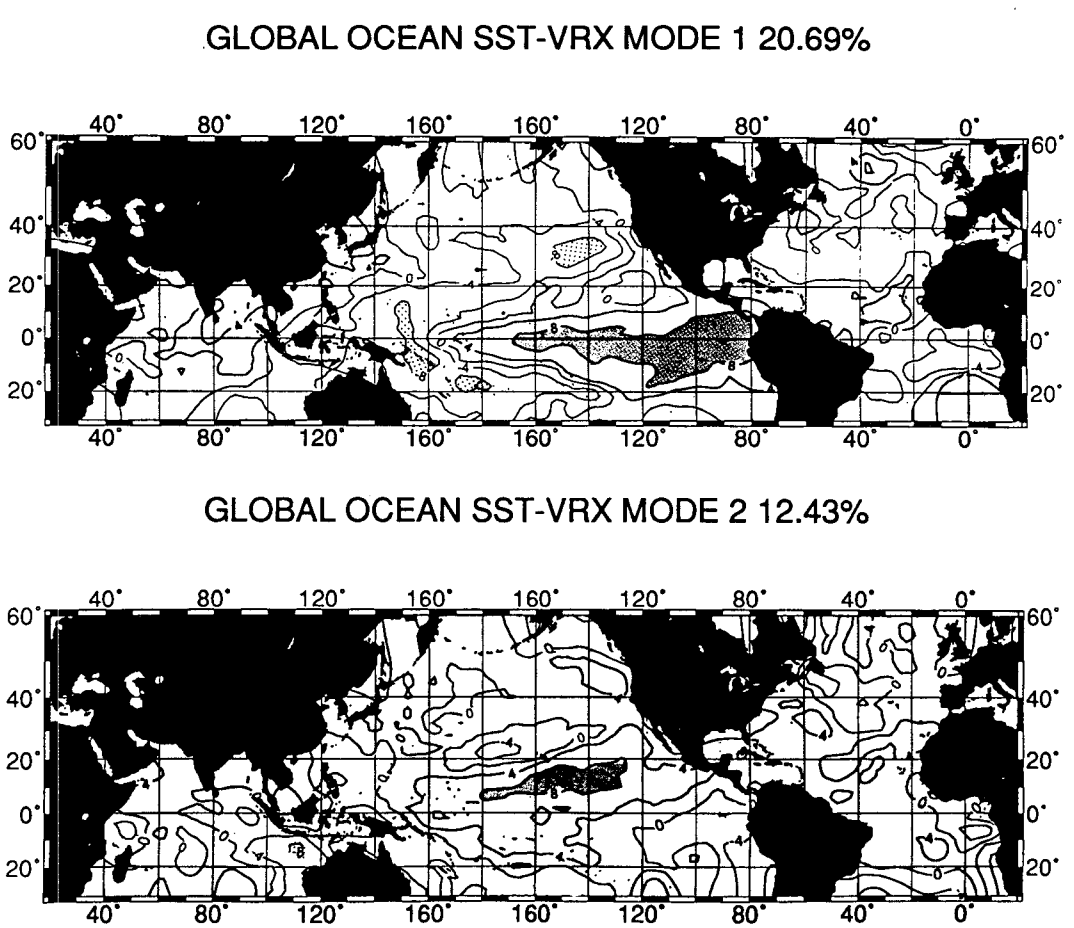

FIG. 16. Spatial patterns (loadings × 10) of the first two VRX modes for SST over the global ocean for the 13-year period 1979–1991. Areas with positive values are shaded. Extrema of the same order of magnitude are either dark shaded (positive) or stippled (negative).

that the loading distribution in the tropical Atlantic may be indicative of the strengthening of the Atlantic southeasterly trades during the El Niño peak phase.

The spatial pattern of the first VRX mode for HS400 over the global ocean (Fig. 17, top) has positive loadings in the eastern equatorial Pacific Ocean. This pattern is nearly identical to that computed for the Pacific Ocean alone. The negative HS400 values in the western equatorial Pacific Ocean are poised to propagate eastward along the equator and terminate the El Niño over the subsequent year's time. Of principal interest are the positive loadings in the western Indian Ocean (compare with Fig. 12, top) and the negative loadings south of Indonesia that match those in the western Pacific Ocean. The tropical Atlantic Ocean represents, to a lesser degree, a structure opposite to its Pacific counterpart with warmer HS400 in the ITCZ area and colder HS400 at the equator and to the southeast at around 10°S.

The spatial pattern of the second VRX mode for SST over the global ocean (Fig. 16, bottom) is dominated by positive loadings, maxima being found off the equator in the Pacific Ocean, that is, poleward of the climatological ITCZ. This is nearly identical to the second EOF mode for the Pacific Ocean alone (Fig. 7, bottom). As mentioned before this pattern represents the precursor SST mode associated with El Niño in the Pacific Ocean. Of principal interest are the small positive SST loadings in the western Indian Ocean, particularly west of 80°E, and the maximum negative loadings south of Indonesia and in the Timor Sea (compare with Fig. 11, bottom), which link with those in the Coral Sea of the western tropical Pacific Ocean. Note also the positive loadings in almost the full Atlantic basin north of 20°S, which go hand in hand with the precursor mode of El Niño in the Pacific Ocean.

The spatial structure of the second EOF mode for HS400 over the global ocean (Fig. 17, bottom) has maximum positive loadings in the central equatorial Pacific Ocean, between the date line and 160°W, extending eastward along the equator. Positive loadings are also found in the northern Pacific between 20°N and 50°N on the eastern flank of the North Pacific gyre. Again this pattern is nearly identical to the pattern

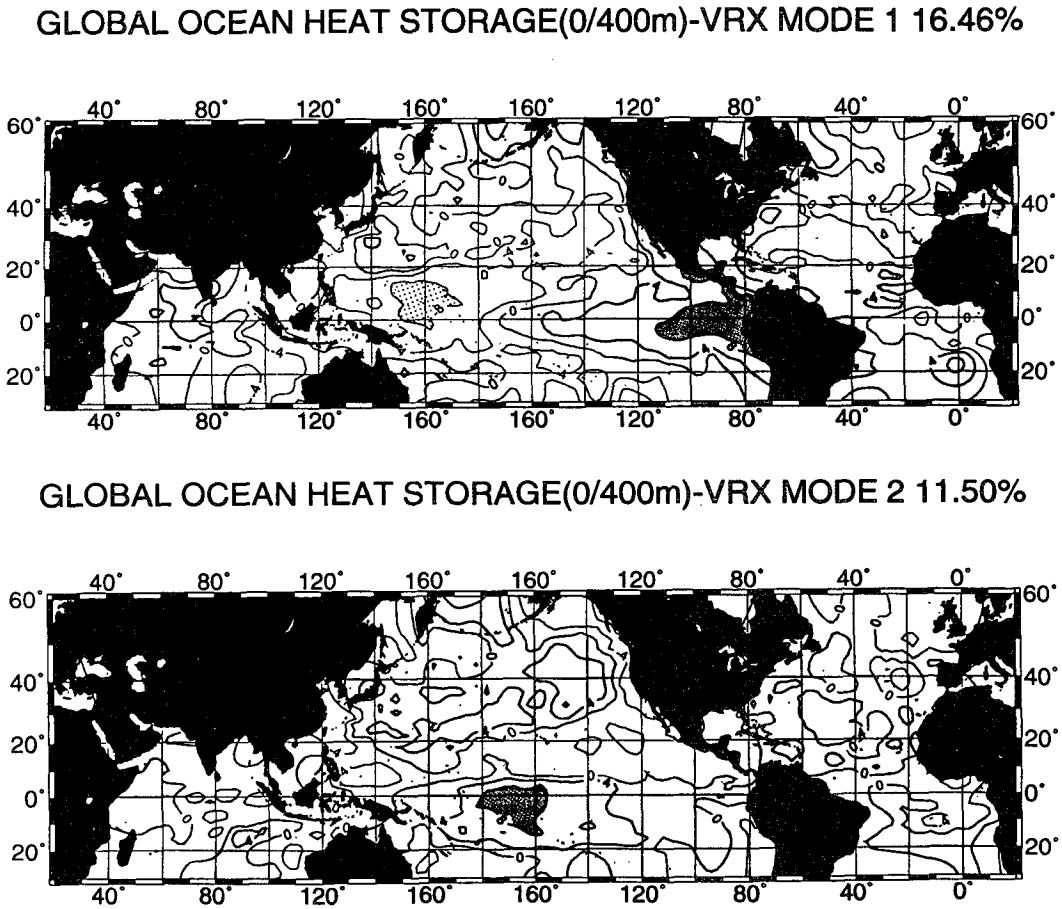

FIG. 17. Spatial patterns (loadings × 10) of the first two VRX modes for HS400 over the global ocean for the 13-year period 1979–1991. Areas with positive values are shaded. Extrema of the same order of magnitude are either dark shaded (positive) or stippled (negative).

computed for the Pacific Ocean alone (Fig. 8, bottom). The negative HS400 values in the western equatorial Pacific Ocean are poised to propagate eastward along the equator and to terminate the El Niño over the subsequent years' time. Of additional interest are the smaller positive loadings found on the eastern flank of the subtropical North Atlantic gyre.

In summary, the first VRX mode for SST anomalies over the global ocean characterizes the peak phase of El Niño off the west coast of South America. In the global tropical band, maximum positive loadings occur in the eastern Pacific Ocean straddling the equator; maximum positive loadings straddle the equator in the central Indian Ocean; while positive loadings are found in the vicinity of the Atlantic ITCZ. The first VRX mode for HS400 anomalies over the global ocean characterize the peak phase of El Niño off the west coast of South America. In the global tropical band, maximum positive loadings occur in the eastern Pacific Ocean straddling the equator extending poleward along the eastern boundary; smaller positive loadings are found in the equatorial Indian Ocean west of 80°E. The second VRX mode for SST over the global ocean is the precursor mode to the first VRX SST mode. It displays positive SST loadings over most of the global ocean, except for the south eastern Indian and western Pacific Oceans. This is very different from the second modes of Nitta and Yamada (1989) and Kawamura (1994). Instead of a precursor mode, their second modes represent a trend in their longer records (1950–1987 and 1955–88, respectively). According to Nitta and Yamada (1989), the tropical SST in the Pacific and Indian Oceans has increased significantly by almost 0.5°C during their analyzed period. Our leading SST modes are similar to the leading EOF modes of a shortwave analysis during approximately the same period (Y. Moisan and P. Niiler 1994, personal communication). This corroborates the eastward and equatorward merging of the deep atmospheric convection during ENSO, associated with the ITCZ and SPCZ. The second VRX mode for HS400 over the global ocean is also the precursor mode to the first VRX HS400 mode. The first and second VRX modes for HS400, taken together, are associated with slow eastward propagation of the ENSO signal along the equator in the Indian and Pacific Oceans. The first and second VRX modes for SST, taken together, on the other hand suggest both eastward propagation and equatorward merging of the anomalies in the Indian and Pacific Oceans. Evidence for propagation in the Atlantic Ocean is unclear.

7. Discussion and conclusions

In the Pacific and Indian Oceans, the two dominant EOF modes in SST and HS400 are associated with the ENSO signal. This is not so in the Atlantic Ocean where the ENSO signal is found only at the surface. The two dominant EOF modes in SST and HS400 associated with the ENSO signal display about the same amount of total variance in each ocean (i.e., 33% and 17% for SST, 24% and 17% for HS400 in the Pacific Ocean; and 31% and 18% for SST, and 21% and 14% for HS400 in the Indian Ocean). Therefore, the ENSO signal in the Indian Ocean explains as much of the interannual variability in that ocean as the ENSO signal does in the Pacific Ocean. In the Atlantic Ocean the ENSO signal accounts at the surface for only 12% of the total interannual variance (SST, third VRX mode). Therefore, the ENSO signal in the Atlantic Ocean is weaker than in the other two oceans and seems to come about as a passive response to an atmosphere that has been initially perturbed in the Indo-Pacific region.

In the Pacific and Indian Oceans, the two dominant EOF modes in SST and HS400 associated with the ENSO signals display similar relationships to each other. For each variable in each ocean, the dominant mode is in phase with the peak phase in El Niño off the west coast of South America, while the second mode or the precursor mode leads the first by at least 6 months. For the Pacific Ocean, this has been known for some time (White et al. 1985) where the spatial structure of the two modes, the second leading the first, is indicative of the slow eastward propagation of the ENSO signal along the equator associated with the evolutionary development of ENSO in this ocean (e.g., Gill and Rasmusson 1983) that culminates in the peak phase of El Niño off the west coast of South America. For the Indian Ocean, the determination of these two modes in SST and HS400 is a new finding. The appearance of the ENSO signal in two EOF modes in the Indian Ocean, one leading the other, also suggests an eastward propagation along the equator (and a south eastward propagation in the eastern Indian Ocean) similar to its better known counterpart in the Pacific Ocean.

A comparison of the EOF modes in the equatorial Pacific and Indian Oceans finds the evolution of the ENSO signal in the Indian Ocean to be different from that in the Pacific Ocean. While warmer SSTs develop in the eastern equatorial Indian Ocean off the west coast of Indonesia at the same time that they form off the west coast of South America during the peak phase of El Niño, these warmer SSTs are not displaced westward of the warmer HS400 as they are in the Pacific Ocean. Rather, they are displaced eastward, with warmer HS400 located in the western and central Indian Ocean. This indicates that dynamical processes that underlie the formation of warmer SST off the west coast of Indonesia are different from those responsible for warmer SST associated with El Niño off the west coast of South America.

It remains to be seen whether a coupled model for the delayed action oscillator for the ENSO signal in the ocean–atmosphere system of the tropical Indian Ocean can be constructed as has been done for the

tropical Pacific Ocean (e.g., Suarez and Schopf 1988). In such an endeavor, an account may need to be taken of the monsoon winds along the east coast of Africa and along the west coast of Indonesia. These alongshore wind stress anomalies may generate significant upwelling and downwelling extremes that can propagate into the interior via Rossby and Kelvin waves, exerting a significant influence upon the ocean–atmosphere interaction there. Certainly, the next step in the statistical study of the ENSO signal in the Indian Ocean is to establish the covariance between zonal and meridional components of the interannual wind stress anomalies and the upper-ocean temperature variability as was accomplished by Graham and White (1988) for the tropical Pacific Ocean.

Whether the ENSO signal in the Indian Ocean has an influence upon the ENSO signal in the Pacific Ocean remains to be tested with coupled models that incorporate both oceans. The global EOF mode displays both SST and HS400 loadings in the eastern Indian Ocean to be in phase with those in the western Pacific Ocean. This suggests that the two domains may be dependent upon each other. Further research is needed before this can be confirmed, not the least of which is to establish whether interannual Kelvin waves can negotiate the multitude of islands that separate the two oceans.

Acknowledgments. Our appreciation extends to the wide range of individuals who, under the auspices of IGOSS and the Intergovernmental Oceanographic Data Exchange (IODE), were instrumental in the collection, transmission, and archival of the temperature–depth observations used in this study. Appreciation is given to Steve Pazan at Scripps Institution of Oceanography (SIO), who conducted scientific quality control of the temperature profiles for the 13-year period of interest. Special thanks to Steve Hong Peng at Lamont-Doherty Earth Observatory (LDEO) and Ted Walker at SIO, who conducted the analyses presented in this study. Our thanks also extend to R. Molinari and to the anonymous reviewers for their extremely helpful comments and suggestions. YMT is partly supported by the Office of Global Programs of NOAA (NOAA 5-3222), while WW is supported by the National Oceanographic Data Center, the National Ocean Service, and the Office of Global Programs of NOAA (NOAA NA 90AA-D-AC416) in concert with the Tropical Ocean–Global Atmosphere (TOGA) Program. Support is also provided by the National Science Foundation (OCE-9196889) in concert with the World Ocean Circulation Experiment (WOCE). Support accrues from the LDEO of the Columbia University, Western Connecticut State University (YMT), and the SIO of the University of California at San Diego (WBW) as well.

REFERENCES

Barnett, T. P., 1983: Interaction of the monsoon and Pacific Trade Wind system at interannual time scales. Part I: The equatorial zone. *Mon. Wea. Rev.*, **111,** 756–773.

——, 1984a: Interaction of the monsoon and Pacific Trade Wind system at the interannual time scales. Part II: The tropics. *Mon. Wea. Rev.*, **112,** 2380–2387.

——, 1984b: Interaction of the monsoon and Pacific Trade Wind system at interannual time scales. Part III: A partial anatomy of the Southern Oscillation. *Mon. Wea. Rev.*, **112,** 2388–2400.

——, 1985: Variations in near-global sea level pressure. *J. Atmos. Sci.*, **42,** 478–501.

Berlage, H. P., 1957: Fluctuations of the general atmospheric circulation of more than one year, their nature and prognostic value. *K. Ned. Meteor. Inst. Meded. Verh.*, **69,** 152 pp.

Bjerknes, J., 1966a: Survey of El Niño 1957–58 in its relation to tropical Pacific meteorology. *Inter.-Amer. Trop. Tuna Comm. Bull.*, **12,** 1–62.

——, 1966b: A possible response of the atmospheric Hadley circulation to equatorial anomalies of ocean temperature. *Tellus*, **18,** 820–829.

——, 1969: Atmospheric teleconnections from the equatorial Pacific. *Mon. Wea. Rev.*, **97,** 163–172.

Carton, J. C., and B. Huang, 1994: Warm events in the tropical Atlantic. *J. Phys. Oceanogr.*, **24,** 888–903.

Davis, J. C., 1973: *Statistics and Data Analysis in Geology.* Wiley & Sons, 550 pp.

Enfield, D. B., 1989: El Niño past and present. *Rev. Geophys.*, **27,** 159–187.

Gandin, L., 1963: *Objective Analysis of Meteorological Fields.* Gidrometeorologicheskoe.

Gill, A. E., and E. Rasmusson, 1983: The 1982–83 climate anomaly in the equatorial Pacific. *Nature,* **306,** 229–234.

Graham, N. E., and W. B. White, 1988: The El Niño cycle: A natural oscillator of the Pacific ocean-atmosphere system. *Science,* **240,** 1293–1302.

Horel, J. D., 1981: A rotated principal component analysis of the interannual variability of the northern hemisphere 500 mb height field. *Mon. Wea. Rev.*, **109,** 2080–2092.

Houghton, R. W., 1991: The relationship of sea surface temperature to thermocline depth at annual and interannual time scales in the tropical Atlantic ocean. *J. Geophys. Res.*, **96,** 15 173–15 185.

——, and C. Colin, 1986: Thermal structures along 4°W in the Gulf of Guinea during 1983–1984. *J. Geophys. Res.*, **91,** 11 727–11 739.

——, and Y. M. Tourre, 1992: Characteristics of low-frequency sea surface temperature fluctuations in the tropical Atlantic. *J. Climate,* **5,** 765–771.

Kaiser, H. F., 1958: The varimax criterion for analytic rotation in factor analysis. *Psychometrika,* **23,** 187–200.

Katz, E. J., 1993: An interannual study of the Atlantic North Equatorial Countercurrent. *J. Phys. Oceanogr.*, **23,** 116–123.

——, P. H. Hisard, J. M. Verstraete, and S. L. Garzoli, 1986: Annual changes of the zonal pressure gradient along the equator of the Atlantic ocean in 1983–1984. *Nature,* **322,** 245–247.

Kawamura, R., 1994: A rotated EOF analysis of global sea surface temperature variability with interannual and interdecadal scales. *J. Phys. Oceanogr.*, **24,** 707–715.

Kaylor, R. E., 1977: Filtering and decimation of digital time series. Tech. Note BN 850, Institute for Physical Science and Technology, University of Maryland, College Park, MD, 22 pp.

Kessler, W. S., 1990: Observations of long Rossby waves in the northern tropical Pacific. *J. Geophys. Res.*, **95,** 5183–5219.

Latif, M., and N. E. Graham, 1992: How much predictive skill is contained in the thermal structure of an OGCM? *J. Phys. Oceanogr.*, **22,** 951–962.

Nitta, T., and S. Yamada, 1989: Recent warming of tropical sea surface temperature and its relationship to the northern hemisphere circulation. *J. Meteor. Soc. Japan,* **67,** 375–383.

North, R. G., T. L. Bell, R. F. Cahalan, and F. J. Hoeng, 1982: Sampling errors in the estimation of empirical orthogonal functions. *Mon. Wea. Rev.*, **110,** 699–706.

Pazan, S., and G. Meyers, 1982: Pacific trade wind fluctuations and the Southern Oscillation index. *Mon. Wea. Rev.*, **110,** 587–600.

Philander, S. G. H., 1986: Unusual conditions in the tropical Atlantic ocean in 1984. *Nature,* **322,** 236–238.

Rasmusson, E. G., and T. H. Carpenter, 1982: Variations in tropical sea surface temperature and surface wind fields associated with the Southern Oscillation/El Niño. *Mon. Wea. Rev.;* **110,** 354–384.

Richman, M. B., 1986: Rotation of principal components. *J. Climatol.,* **6,** 293–335.

Ropelewski, C. F., and M. S. Halpert, 1992: Observed tropospheric biennial variability and its relationship to the southern oscillation. *J. Climate,* **5,** 594–614.

Shopf, P. S., and M. J. Suarez, 1988: Vacillations in a coupled ocean–atmosphere model. *J. Atmos. Sci.,* **45,** 549–566.

Suarez, M. J., and P. S. Shopf, 1988: A delayed action oscillator for ENSO. *J. Atmos. Sci.,* **45,** 3283–3287.

White, W. B., G. Meyers, J. R. Donguy, and S. E. Pazan, 1985: Short-term climatic variability of the Pacific Ocean during 1979–82. *J. Phys. Oceanogr.,* **15,** 917–935.

——, S. E. Pazan, and M. Inoue, 1987: Hindcast–forecast of ENSO events based upon the redistribution of observed and model heat content in the western tropical Pacific. *J. Phys. Oceanogr.,* **17,** 264–280.

Wyrtki, K., 1989: Some thoughts about the west Pacific warm pool. *Proc. W. Pac. Int. Meeting and Workshop on TOGA COARE.* J. Picaut, R. Lukas, and T. Delcroix, Eds., Noumea, New Caledonia, ORSTROM 99–109.

Yasunari, T., 1985: Zonally propagating modes of the global east-west circulation associated with the Southern Oscillation. *J. Meteor. Soc. Japan,* **63,** 1013–1029.

——, 1987: Global structure of the El Niño/Southern Oscillation. Part II. Time evolution. *J. Meteor. Soc. Japan,* **65,** 81–10.

Zebiak, S., 1993: Air–sea interaction in the equatorial Atlantic regions. *J. Climate,* **6,** 1567–1586.

——, and M. A. Cane, 1987: A model El Niño–Southern Oscillation. *Mon. Wea. Rev.,* **115,** 2262–2278.